Nanoscale Research Letters

NANO EXPRESS Open Access

Tunable and Anisotropic Dual-Band Metamaterial Absorber Using Elliptical Graphene-Black Phosphorus Pairs

Yijun Cai[1], Shuangluan Li[2], Yuanguo Zhou[2*], Xuanyu Wang[1], Kai-Da Xu[3], Rongrong Guo[1] and William T. Joines[4]

Abstract

We numerically propose a dual-band absorber in the infrared region based on periodic elliptical graphene-black phosphorus (BP) pairs. The proposed absorber exhibits near-unity anisotropic absorption for both resonances due to the combination of graphene and BP. Each of the resonances is independently tunable via adjusting the geometric parameters. Besides, doping levels of graphene and BP can also tune resonant properties effectively. By analyzing the electric field distributions, surface plasmon resonances are observed in the graphene-BP ellipses, contributing to the strong and anisotropic plasmonic response. Moreover, the robustness for incident angles and polarization sensitivity are also illustrated.

Keywords: Metamaterial absorber, Two-dimensional material, Dual-band absorber, Surface plasmons

Introduction

Graphene is a two-dimensional material with carbon atoms arranged in a honeycomb lattice [1, 2]. Various graphene-based photonic devices have been developed in the recent years due to their ultracompact size and unique light-graphene interaction [3–6]. As one of its most significant applications, metamaterial absorbers based on graphene have attracted burgeoning amount of interest due to their strong and tunable plasmonic response [7–10]. However, several applications that require high on-off ratio are restricted due to the zero or near-zero band gap of graphene [11]. As an alternative two-dimensional material, black phosphorus (BP), a monolayer of phosphorus atoms arranged in a hexagonal lattice with a puckered structure [12], has also received a surge of research interest recently. It possesses exceptional optical and electronic properties, such as in-plane anisotropy, thickness-dependent tunable band gap [13], and high carrier density and mobility [14]. Over the past few years, in the infrared region, researchers have investigated numerous structures to enhance the light-BP interaction strength in the metamaterial based on BP [15–17]. Nevertheless, the plasmonic resonance of BP-based absorber is hardly to be tuned flexibly and effectively, and they normally suffer from relatively low absorption rate with moderate doping level. This is attributed to the fact that the resonance strength in monolayer BP is rather weak, limiting its anisotropic potentials. Thus, graphene-BP-based plasmonic absorbers have been proposed utilizing the hybridization of graphene and BP to achieve strong and anisotropic plasmonic absorption [18–20]. However, the previous reported graphene-BP-based absorbers generally require relatively complicated fabrication technique or possess single absorption band, impeding their further applications for imaging, biosensing, and communication systems.

In our work, an anisotropic dual-band infrared absorber is numerically proposed using periodic elliptical graphene-BP pairs, which is ease of fabrication. The independent tunability of resonance by geometric size and doping level is demonstrated. Electric field distributions are plotted to reveal the physical mechanism. The incident angle tolerance and polarization sensitivity are also illustrated.

* Correspondence: wingkoo@foxmail.com
[2]College of Communication and Information Engineering, Xi'an University of Science and Technology, Xi'an 710054, China
Full list of author information is available at the end of the article

Methods

The proposed absorber is made up of transverse and longitudinal elliptical graphene-BP pairs deposited on a SiO_2 layer as shown in Fig. 1. A hexagonal boron nitride (hBN) layer is inserted between monolayer graphene and BP as an insulating spacer to prevent carrier transport between them and guarantee high carrier mobility. The parameters of SiO_2 and hBN are obtained from Ref. 21 and Ref. 22 respectively. The simulations are carried out by COMSOL Multiphysics to investigate the dual-band properties, which is based on finite element method (FEM) in the frequency domain. We apply Floquet periodicity as the boundary conditions in both *x*- and *y*- directions. A port with infrared wave excitation is set upon the top surface of the computational domain, while perfect electric conductor (PEC) boundary condition is set on the bottom surface. Tetrahedral meshes with user-controller mesh density are applied for the entire domain.

In the simulation, both graphene and BP are treated as two-dimensional surface with surface conductivities instead of bulk materials with permittivity tensors. This assumption solves the problems of thickness definition for ultrathin materials and low computational efficiency [23].

To describe the surface conductivity of graphene $\sigma(\omega)$, we use the well-known Kubo formulas as below [24]:

$$\sigma(\omega,\mu_c,\Gamma,T)=\sigma_{\text{intra}}+\sigma_{\text{inter}} \tag{1}$$

$$\sigma_{\text{intra}}=\frac{je^2}{\pi\hbar^2(\omega-j2\Gamma)}\times\int_0^{\infty}\xi\left(\frac{\partial f_d(\xi,\mu_c,T)}{\partial\xi}-\frac{\partial f_d(-\xi,\mu_c,T)}{\partial\xi}\right)d\xi \tag{2}$$

$$\sigma_{\text{inter}}=-\frac{je^2(\omega-j2\Gamma)}{\pi\hbar^2}\times\int_0^{\infty}\frac{f_d(-\xi,\mu_c,T)-f_d(\xi,\mu_c,T)}{(\omega-j2\Gamma)^2-4(\xi/\hbar)^2}d\xi \tag{3}$$

$$f_d(\xi,\mu_c,T)=\left(e^{(\xi-\mu_c)/k_BT}+1\right)^{-1} \tag{4}$$

According to Eq. 1, $\sigma(\omega)$ consists of the intraband and interband counterparts, namely σ_{intra} and σ_{inter}. ω is the radian frequency, μ_c is the chemical potential, Γ is the scattering rate, and T is the Kelvin temperature. $\hbar$, e, ξ, and k_B are the reduced Planck constant, electron charge, electron energy, and Boltzmann constant, respectively.

In the infrared region, since the incident photon can hardly excite the interband transition, the light-graphene interaction is dominated by the intraband transition. Particularly, when $\mu_c \gg k_BT$, Kubo formulas can be further simplified to Eq. 5:

$$\sigma_g=\frac{ie^2\mu_c}{\pi\hbar^2(\omega+i2\Gamma)} \tag{5}$$

Thus, the surface conductivity of graphene is dependent on the values of ω, Γ, and μ_c. Here, Γ is assumed as 0.3 meV and μ_c is assumed to be 0.7 eV according to the previous work [25, 26].

On the other hand, we calculate the surface conductivity σ_j of BP with a simple semi-classical Drude model [27]:

$$\sigma_j=\frac{iD}{\pi\left(\omega+\frac{i\Gamma_{\text{BP}}}{\hbar}\right)} \tag{6}$$

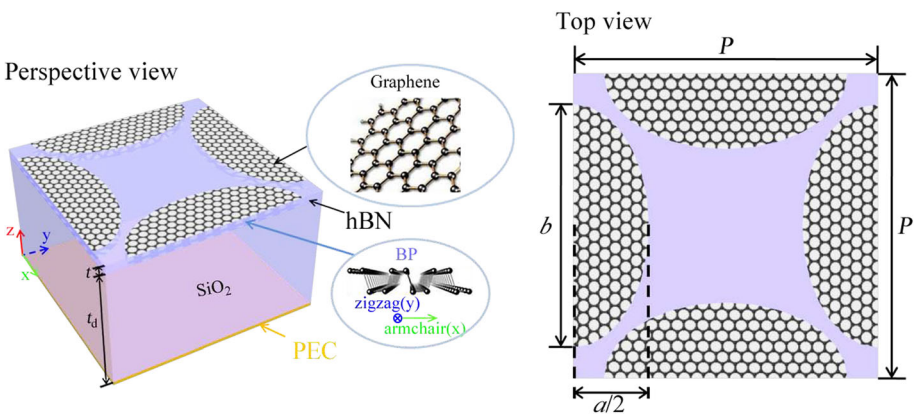

Fig. 1 A unit cell of the proposed absorber based on elliptical graphene-BP pairs. t_d and t are the thicknesses of the dielectric and insulator layer, respectively. *a* and *b* are the short axis and long axis of the ellipse. *P* is the periodic side length of the square unit cell

$$D_j = \frac{\pi e^2 n_s}{m_j} \tag{7}$$

where n_s is the carrier density relating with the doping level. We choose $n_s = 1.9 \times 10^{13}\,\mathrm{cm}^{-2}$ and $\Gamma_{BP} = 10\,\mathrm{meV}$ according to the previous reference [16]. j is the concerned direction, so σ_x and σ_y are determined by the electron mass along x- and y-direction, respectively. m_x and m_y can be further calculated by:

$$m_x = \frac{\hbar^2}{\frac{2\gamma^2}{\Delta} + \eta_c} \tag{8}$$

$$m_y = \frac{\hbar^2}{2v_c} \tag{9}$$

$$\eta_c = \frac{\hbar^2}{0.4m_0} \tag{10}$$

$$v_c = \frac{\hbar^2}{1.4m_0} \tag{11}$$

$$\gamma = \frac{4a}{\pi} \tag{12}$$

where m_0 is the standard electron mass, and Δ and a are the band gap and scale length for BP monolayer, respectively. By substituting Eqs. 10–12 into Eq. 8 and Eq. 9, one can obtain the electron mass along armchair (x-) and zigzag (y-) direction. The discrepancy between them contributes to the anisotropic surface conductivity of BP.

Results and Discussion

To illustrate the anisotropic absorption characteristic of the proposed absorber, we first simulate and compare the absorption spectra with individual graphene layer, individual BP layer, and graphene-BP pairs. As can been observed in Fig. 2a, the plasmonic response of graphene

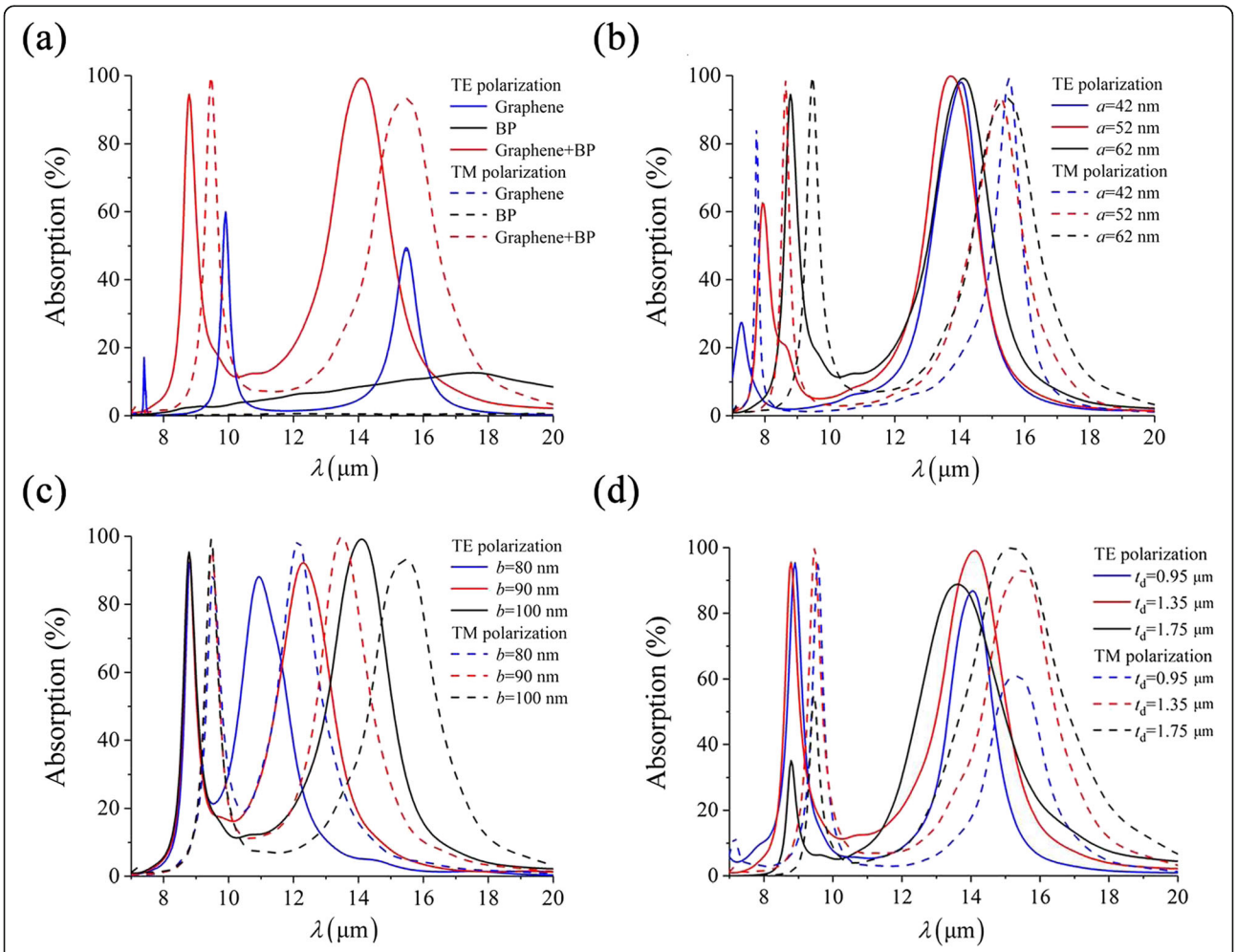

Fig. 2 a Comparison of plasmonic responses between monolayer graphene (blue solid curve and blue dashed curve are overlapped), monolayer BP and graphene-BP pairs, and absorption spectra with different a (**b**), b (**c**), and t_d (**d**). The default parameters are $a = 62$ nm, $b = 100$ nm, $t_d = 1.35$ μm, $t = 5$ nm, and $P = 250$ nm, under normal incidence

is isotropic with two obvious absorption peaks at 9.9 μm and 15.4 μm, independent on the polarization. On the other hand, although the plasmon resonance of BP is anisotropic, its strength is quite weak for either TE (< 12.7%) or TM (< 0.7%) incidence. By combining the advantages of graphene and BP, graphene-BP pairs exhibit both strong and anisotropic plasmonic responses. For TE incidence, the two absorption peaks are located at 8.8 μm and 14.1 μm, with absorption rates larger than 90%. For TM incidence, the wavelengths of maximum absorption are shifted to 9.5 μm and 15.4 μm, respectively. The polarization extinction ratio can be defined as $PER = 10 \times \log(R_1/R_0)$, where R_1 and R_0 denote the reflectance ($R = 1\text{-}A$, A represents the absorbance) of different polarizations at the same wavelength, then the maximum PER of each resonance can reach up to 23 dB and 25 dB at $\lambda = 9.5$ μm and $\lambda = 14.1$ μm, respectively. Therefore, the proposed absorber can be utilized as a dual-band reflective polarizer with high performance.

We next analyze the absorption spectra with different geometric configurations to demonstrate the tunable dual-band absorption property in Fig. 2b–d. In Fig. 2b, the first absorption peaks have redshifts as a increases from 42 to 52 nm for both polarizations, while second resonant frequencies are almost unchanged. On the other hand, as shown in Fig. 2c, by increasing the long axis length b, the second resonances are redshifted as well, while the first absorption peaks remain constant for TE and TM polarization. Therefore, the dual absorption peaks can be tuned independently by varying the corresponding axis length in the elliptical graphene-BP pairs. Moreover, the thickness of dielectric layer also plays a critical role in the performance for the proposed device, which acts as a Fabry-Perot resonator formed by the graphene-BP metasurface and the PEC substrate. Thus, the absorption spectra with different t_d are plotted in Fig. 2d. As t_d increases from 0.95 to 1.75 μm, the first absorption peaks for TE and TM polarization have a dramatic drop, while the second peaks increase at first then decrease sharply. As a consequence, there is an optimal thickness t_d that maximizes the dual absorption peaks of the proposed absorber.

In order to elucidate the physical insight, we further reveal the electric field intensity distributions at different wavelengths in Fig. 3. For TE incidence, the electric field is in the armchair (x-) direction. At the first peak (λ = 8.8 μm), the incident infrared light can excite electrons in graphene and BP to oscillate in the transverse direction, leading to the concentration of electric field at the short axis ends of the longitudinal ellipse as shown in Fig. 3a. At $\lambda = 14.1$ μm, the localized electric field is enhanced at the long axis ends of the transverse ellipse. On the other hand, TM incidence with electric field in the zigzag (y-) direction can excite electrons to vibrate

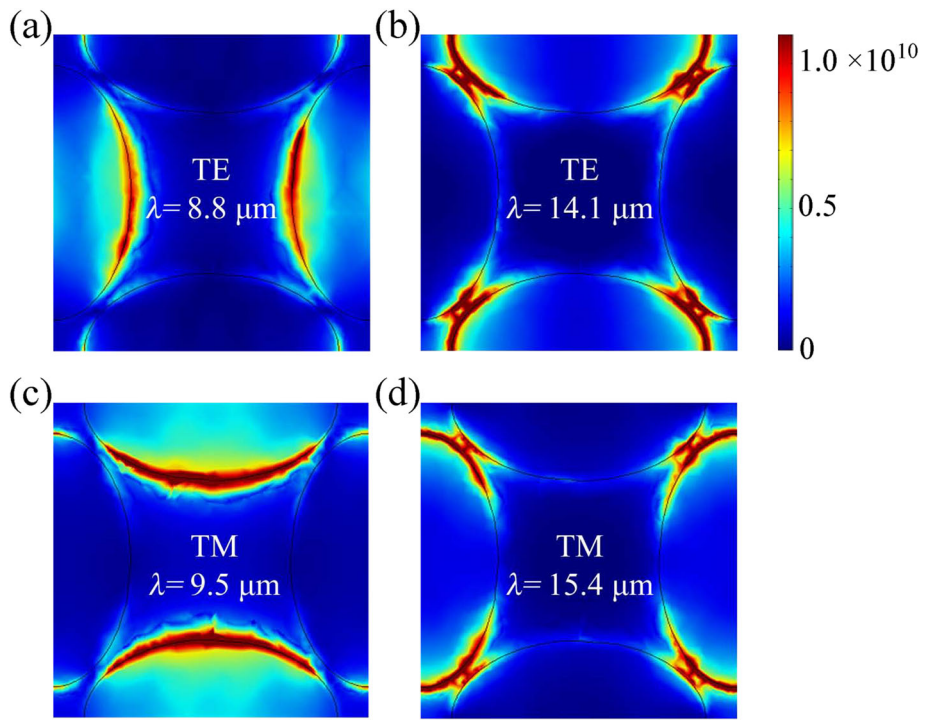

Fig. 3 Electric field intensity distributions at different wavelengths for **a**, **b** TE and **c**, **d** TM polarization, where $a = 62$ nm, $b = 100$ nm, $t_d = 1.35$ μm, $t = 5$ nm, $P = 250$ nm, under normal incidence

along the longitudinal direction at the absorption peak of 9.5 μm, leading to concentrated field distributions at the short axis ends of the transverse ellipse. Besides, at λ = 15.4 μm, the enhancement of electric field is focused at the long axis ends of the longitudinal ellipse. Therefore, the resonance wavelengths are directly related to the finite oscillation length of the induced dipoles in both transverse and longitudinal elliptical graphene and BP pairs.

One can tune the anisotropic dual-band absorption performance effectively by varying the geometric dimensions as demonstrated in Fig. 2b–d. Meanwhile, the surface conductivities of graphene and BP can also be manipulated by varying μ_c and n_s according to graphene and BP model formulas as mentioned above. μ_c and n_s represent the doping level of graphene and BP that can be altered after geometric fabrication. Thus, performances of the proposed absorber with different μ_c and n_s are depicted in Fig. 4. Considering the practical situation, μ_c is chosen between 0.4 and 0.8 eV from the previous work verified by experiments [28]. In the previous reported work [29], the maximum theoretical value for n_s of BP was demonstrated to be $2.6 \times 10^{14}\,\mathrm{cm}^{-2}$, so a moderate n_s is chosen between $10^{13}\,\mathrm{cm}^{-2}$ and $10^{14}\,\mathrm{cm}^{-2}$ in the simulation. In Fig. 4a, when $\mu_c = 0.4$ eV, the first absorption peak is located at 10.9 μm and the second one is located at 17.1 μm. As μ_c increases to 0.8 eV, the two resonant wavelengths are blueshifted to 8.4 μm and 13.4 μm. Similarly for TM polarization, the dual absorption peaks are blueshifted from 12.4 and 19.8 μm to 8.9 and 14.4 μm, respectively, with μ_c increasing from 0.4 to 0.8 eV as shown in Fig. 4b. For individual patterned BP, the resonance wavelength λ_p can be calculated as $\lambda_p \propto \sqrt{L/n_s}$, where L is the effective oscillation length [27]. Thus, if L is fixed, the absorption spectra exhibit an obvious blueshift as n_s increases for TE polarization as plotted in Fig. 4c. For TM polarization, the absorption peaks are also slightly blueshifted as n_s increases from $10^{13}\,\mathrm{cm}^{-2}$ to $10^{14}\,\mathrm{cm}^{-2}$ as demonstrated in Fig. 4d.

In the practical applications, tolerance of wide incident angles is preferred for infrared absorbers. Therefore, absorption spectra under oblique incidences are elaborated. In Fig. 5a, it is observed that, for TE polarization, the first absorption peak remains larger than 80% when θ increases to 52°, while the second absorption peak maintains above 80% even when θ increases to 80°. When $\theta >$ 46°, the second resonant wavelength is redshifted

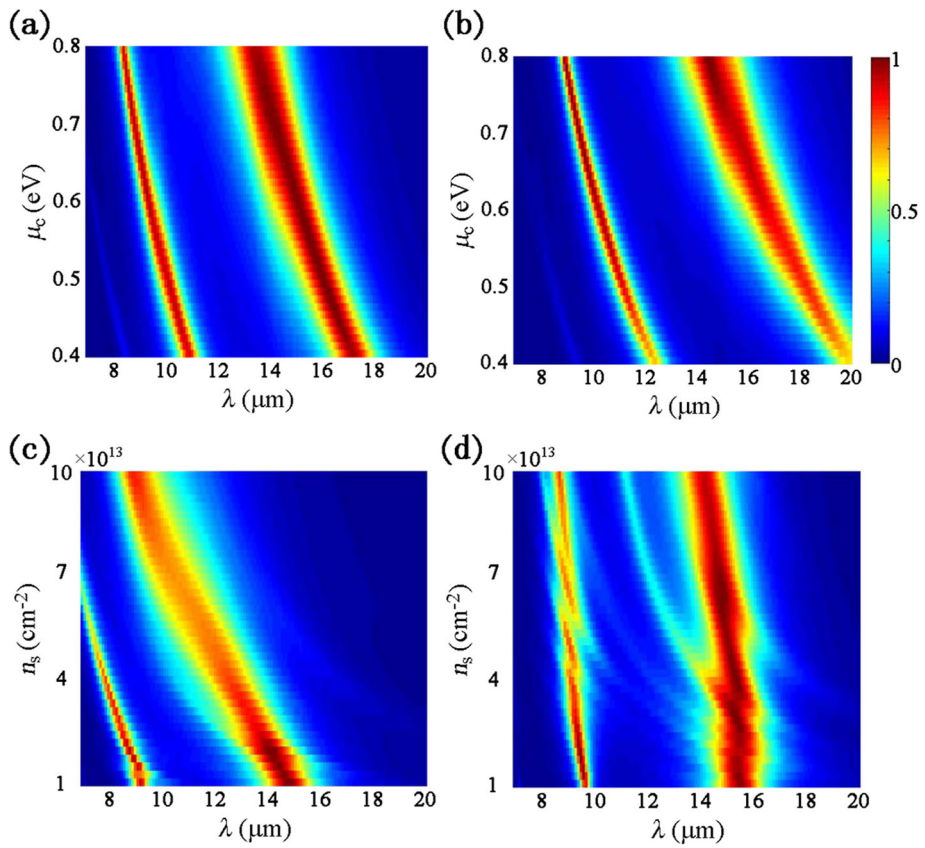

Fig. 4 Absorption spectra versus different doping levels under normal incidence: **a** and **b** for varied chemical potentials of graphene, **c** and **d** for varied carrier densities of BP, **a** and **c** for TE polarization, and **b** and **d** for TM polarization, where $a = 62$ nm, $b = 100$ nm, $t_d = 1.35$ μm, $t = 5$ nm, and $P = 250$ nm

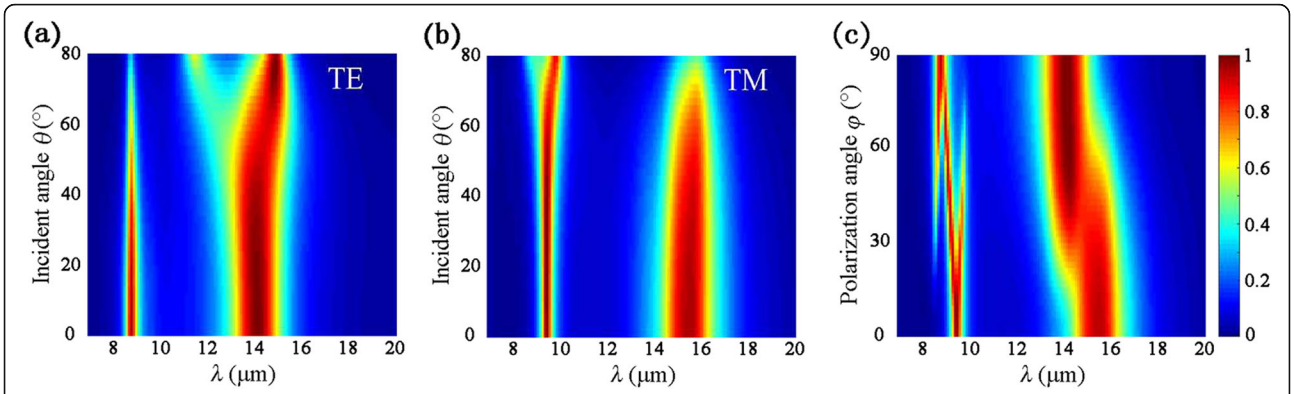

Fig. 5 Absorption spectra under various incident angles for **a** TE and **b** TM polarization and **c** various polarization angles under normal incidence. Geometric parameters are the same as in Fig. 4

gradually as θ becomes larger. For TM incidence, when θ is less than 62°, the absorption rate at the first peak maintains larger than 90%, while the resonant wavelength keeps constant at $\lambda = 9.5$ μm as shown in Fig. 5b. Besides, for the second resonance, the peak absorption remains larger than 80% with θ up to 60°, then drops slightly with the increase of θ. The excellent angular stability originates from the common feature of Fabry-Perot resonators, which are robust for oblique incident angles [30].

Absorption spectra under normal incidence with different polarization angles ϕ are presented in Fig. 5c to investigate the polarization dependence of the proposed absorber. We assume the polarization angle of TE polarization to be 0°. One can see from Fig. 5c that, as ϕ increases from 0 to 90°, the absorption spectrum turns out to be the same as the TM polarization in Fig. 2a. When $0° < \phi < 90°$, the incidence will excite electrons in BP to oscillate in both armchair and zigzag directions due to its x- and y- components of the incident electric field. Consequently, surface plasmon resonances can be induced simultaneously in armchair and zigzag directions of BP.

Conclusions

In conclusions, we have proposed an anisotropic dual-band infrared absorber consisting of periodic transverse and longitudinal graphene-BP ellipses. The maximum PER at each resonance can reach up to 23 dB and 25 dB. The dual anisotropic resonances are attributed to the induced electric dipoles located at the ends of short and long axes. By adjusting the lengths of short axis and long axis, the first and second absorption peaks can be independently tuned, respectively. Moreover, the resonant absorption bands can also be tuned by changing the corresponding doping level of graphene and BP. Besides, high absorption rates at both peaks can be achieved under oblique incidence for any polarization. The proposed absorber can be utilized as a tunable reflective polarizer and novel infrared sensor.

Abbreviations

BP: Black phosphorus; FEM: Finite element method; hBN: Hexagonal boron nitride; PEC: Perfect electric conductor; TE: Transverse electric; TM: Transverse magnetic

Authors' Contributions

CY and LS conceived the idea and wrote the manuscript. ZY and WX undertook the simulations. XK analyzed the data. GR and JW supervised the project. All authors read and approved the final manuscript.

Funding

This work was supported by the National Natural Science Foundation of China (51702271), the Young and Middle-aged Teachers Education and Scientific Research Foundation of Fujian Province, China (JAT170407), and the High Level Talent Project of Xiamen University of Technology, China (YKJ16016R).

Availability of Data and Materials

All data are fully available without restriction.

Competing Interests

The authors declare that they have no competing interests.

Author details

[1]Fujian Provincial Key Laboratory of Optoelectronic Technology and Devices, Xiamen University of Technology, Xiamen 361024, China. [2]College of Communication and Information Engineering, Xi'an University of Science and Technology, Xi'an 710054, China. [3]Department of Electrical and Computer Engineering, University of Wisconsin–Madison, Madison, WI 53706, USA. [4]Department of Electrical and Computer Engineering, Duke University, Durham, NC 27708, USA.

Received: 24 August 2019 Accepted: 10 October 2019
Published online: 21 November 2019

References

1. Novoselov KS, Geim AK, Morozov SV, Jiang D, Zhang Y, Dubonos SV, Grigorieva IV, Firsov AA (2004) Electric field effect in atomically thin carbon films. Science 306:666–669
2. Geim AK, Novoselov KS (2007) The rise of graphene. Nat Mater 6:183–191
3. Li H, Wang L, Zhang H, Huang Z, Sun B, Zhai X, Wen S (2014) Graphene-based mid-infrared, tunable, electrically controlled plasmonic filter. Appl Phys Express 7:024301
4. Cai Y, Zhu J, Liu QH (2015) Tunable enhanced optical absorption of graphene using plasmonic perfect absorbers. Appl Phys Lett 106:043105
5. Wu B, Zu H, Xue B, Zhao Y, Cheng QS (2019) Flexible wideband power divider with high isolation incorporating spoof surface plasmon polaritons transition with graphene flake. Appl Phys Express 12:022008
6. Cai Y, Xu KD, Guo R, Zhu J, Liu QH (2018) Graphene-based plasmonic tunable dual-band bandstop filter in the far-infrared region. IEEE Photonics J 10:5900709

7. Xiao S, Wang T, Liu Y, Xu C, Han X, Yan X (2016) Tunable light trapping and absorption enhancement with graphene ring arrays. Phys Chem Chem Phys 18:26661–26669
8. Cai Y, Xu KD (2018) Tunable broadband terahertz absorber based on multilayer graphene-sandwiched plasmonic structure. Opt Express 26: 31693–31705
9. Zhang K, Yuan Y, Ding X, Ratni B, Burokur SN, Wu Q (2019) High-efficiency metalenses with switchable functionalities in microwave region. ACS Appl Mater Interfaces 11:28423–28430
10. Yuan Y, Zhang K, Ding X, Ratni B, Burokur SN, Wu Q (2019) Complementary transmissive ultra-thin meta-deflectors for broadband polarization-independent refractions in the microwave region. Photonic Res 7:80–88
11. Chen Y, Jiang G, Chen S, Guo Z, Yu X, Zhao C, Zhang H, Bao Q, Wen S, Tang D, Fan D (2015) Mechanically exfoliated black phosphorus as a new saturable absorber for both Q-switching and mode-locking laser operation. Opt Express 23:12823–12833
12. Liu H, Neal AT, Zhu Z, Luo Z, Xu X, Tomanek D, Ye PD (2014) Phosphorene: an unexplored 2D semiconductor with a high hole mobility. ACS Nano 8: 4033–4041
13. Li L, Yu Y, Ye GJ, Ge Q, Ou X, Wu H, Feng D, Chen XH, Zhang Y (2014) Black phosphorus field-effect transistors. Nat Nanotechnol 9:372–377
14. Saito Y, Iwasa Y (2015) Ambipolar insulator-to-metal transition in black phosphorus by ionic-liquid gating. ACS Nano 9:3192–3198
15. Liu Z, Aydin K (2016) Localized surface plasmons in nanostructured monolayer black phosphorus. Nano Lett 16:3457–3462
16. Wang J, Jiang Y (2017) Infrared absorber based on sandwiched two-dimensional black phosphorus metamaterials. Opt Express 25:5206–5216
17. Qing YM, Ma HF, Tie JC (2018) Strong coupling between magnetic plasmons and surface plasmons in a black phosphorus-spacer-metallic grating hybrid system. Opt Lett 43:4985–4988
18. Nong J, Wei W, Wang W, Lan G, Shang Z, Yi J, Tang L (2018) Strong coherent coupling between graphene surface plasmons and anisotropic black phosphorus localized surface plasmons. Opt Express 26:1633–1644
19. Hong Q, Xiong F, Xu W, Zhu Z, Liu K, Yuan X, Zhang J, Qin S (2018) Towards high performance hybrid two-dimensional material plasmonic devices: strong and highly anisotropic plasmonic resonances in nanostructured graphene-black phosphorus bilayer. Opt Express 26: 22528–22535
20. Cai Y, Xu KD, Feng N, Guo R, Lin H, Zhu J (2019) Anisotropic infrared plasmonic broadband absorber based on graphene-black phosphorus multilayers. Opt Express 27:3101–3112
21. Palik ED (1998) Handbook of optical constants of solids, vol 3. San Diego: Academic, p 207
22. Ishii T, Sato T (1983) Growth of single crystals of hexagonal boron nitride. J Cryst Growth 61:689–690
23. Zhu J, Cheng J, Zhang L, Liu QH (2017) Modeling of 2D graphene material for plasmonic hybrid waveguide with enhanced near-infrared modulation. Mater Lett 186:53–56
24. Hanson GW (2008) Dyadic Green's functions and guided surface waves for a surface conductivity model of graphene. J Appl Phys 103:064302
25. Diaz J, Morote M, Carrier J (2013) Plane wave excitation-detection of non-resonant plasmons along finite-width graphene strips. Opt Express 21: 24856–24872
26. Ye L, Sui K, Liu Y, Zhang M, Liu QH (2018) Graphene-based hybrid plasmonic waveguide for highly efficient broadband mid-infrared propagation and modulation. Opt Express 26:15935–15947
27. Low T, Roldán R, Wang H, Xia F, Avouris P, Moreno LM, Guinea F (2014) Plasmons and screening in monolayer and multilayer black phosphorus. Phys Rev Lett 113:106802
28. Jiang Y, Zhang H, Wang J, Gao C, Wang J, Cao W (2018) Design and performance of a terahertz absorber based on patterned graphene. Opt Lett 43:4296–4299
29. Luo Z, Liu M, Guo Z, Jiang X, Luo A, Zhao C, Yu X, Xu W, Zhang H (2015) Microfiber-based few-layer black phosphorus saturable absorber for ultra-fast fiber laser. Opt Express 23:20030–20039
30. Luo X, Zhai X, Wang L, Lin Q (2018) Enhanced dual-band absorption of molybdenum disulfide using a plasmonic perfect absorber. Opt Express 26: 11658–11666

Publisher's Note